Deletion of Socs3 in LysM+ Cells and Cx3cr1 Resulted in Age-dependent Development of Retinal Microgliopathy

Xuan Du
The Wellcome-Wolfson Institute for Experimental Medicine, School of Medicine, Dentistry & Biomedical Sciences, Queen's University Belfast, Northern Ireland, UK

Rosana Penalva
The Wellcome-Wolfson Institute for Experimental Medicine, School of Medicine, Dentistry & Biomedical Sciences, Queen's University Belfast, Northern Ireland, UK

Karis Little
The Wellcome-Wolfson Institute for Experimental Medicine, School of Medicine, Dentistry & Biomedical Sciences, Queen's University Belfast, Northern Ireland, UK

Adrien Kissenpfennig
The Wellcome-Wolfson Institute for Experimental Medicine, School of Medicine, Dentistry & Biomedical Sciences, Queen's University Belfast, Northern Ireland, UK

Mei Chen
The Wellcome-Wolfson Institute for Experimental Medicine, School of Medicine, Dentistry & Biomedical Sciences, Queen's University Belfast, Northern Ireland, UK

Heping Xu (heping.xu@qub.ac.uk)
The Wellcome-Wolfson Institute for Experimental Medicine, School of Medicine, Dentistry & Biomedical Sciences, Queen's University Belfast, Northern Ireland, UK https://orcid.org/0000-0003-4000-931X

Research article

Keywords: Aging, primary microglial dysfunction, retinal degeneration, microgliopathy, neuroinflammation, neuron-microglial interaction, cytokines, chemokines

Posted Date: August 10th, 2020

DOI: https://doi.org/10.21203/rs.3.rs-47513/v1

Version of Record: A version of this preprint was published on February 18th, 2021. See the published version at https://doi.org/10.1186/s13024-021-00432-9.

Abstract

Background

We generated a mouse model of primary microglial dysfunction by deleting two negative immune regulatory genes, *Cx3cr1* and *Socs3* (in LysM$^+$ cells). This study aimed to understand how primary microglial dysfunction impacts retinal neurons during aging.

Methods

The *LysMCre-Socs3*$^{fl/fl}$*Cx3cr1*$^{gfp/gfp}$ double knockout (DKO), *LysMCre-Socs3*$^{fl/fl}$, *Cx3cr1*$^{gfp/gfp}$ and *Socs3*$^{fl/fl}$ mice were maintained up to 12 months. Eyes were collected and processed for immunohistochemistry of IBA-1, cone arrestin, secretagogin, PKCα and GABA. Brain microglia from DKO and WT mice were stimulated with LPS + IFNγ or IL4. The expression of TNFα, IL1β, IL6, iNOS, IL12p40, IL23p19, CCL2, CCL5, CXCL2, IL10, CD206 and Arg1 were examined by real-time RT-PCR and protein production was measured by Luminex assay. Retinal explants from C57BL/6J mice were co-cultured with microglia from DKO or WT mice for 24 h, after which the number of cone arrestin$^+$ cells in retinal flatmount were quantified.

Results

In 3–5 month old mice, the number of microglia in retinal ganglion cell layer (GCL) and inner plexiform layer (IPL) were comparable in all strains. The DKO mice had a significantly higher number of microglia in the outer plexiform layer (OPL) but significantly lower numbers of cone arrestin$^+$, secretagogin$^+$ and GABA$^+$ cells compared to *Socs3*$^{fl/fl}$ and single KO mice. During aging, 57% of the DKO mice died before 12 months old. The 10–12 months old DKO mice had significantly highers number of microglia in GCL/IPL and OPL than age-matched *Socs3*$^{fl/fl}$ and single KO mice. The aged DKO mice developed retinal pigment epithelial (RPE) dysmorphology accompanied by subretinal microglial accumulation. The number of photoreceptors, bipolar cells (Secretagogin$^+$ or PKCα$^+$) and GABA$^+$ amacrine cells was significantly lower in aged DKO mice compared to age-matched *Socs3*$^{fl/fl}$ and single KO mice. Microglia from DKO mice showed significantly higher levels of phagocytic activity and produced higher levels of TNFα, IL6, CCL2, CCL5, CXCL2 and CXCL10 compared to microglia from *Socs3*$^{fl/fl}$ mice. Co-culture of retinal explants with DKO microglia (pre-treated with LPS + IFNγ or IL4) significantly reduced cone photoreceptor survival.

Conclusions

The *LysMCre-Socs3*$^{fl/fl}$*Cx3cr1*$^{gfp/gfp}$ DKO mice displayed primary microglial dysfunction and developed age-related retinal microgliopathy characterized by aggragated microglial activation and multiple retinal neuronal and RPE degeneration.

Trial registration: Not applicable. The article does not contain any results from human participants.

Background

Microglia, the resident innate immune cells of the central nervous system (CNS), which includes the retina, play an important role in safeguarding neurons from exogenous and endogenous insults (1–3). Microglia can detect damage-associated molecular patterns (DAMPs) released by diseased neurons or pathogen-associated molecular patterns (PAMPs) from invading microbes with pattern recognition receptors (PRRs) such as toll-like receptors (TLRs), NOD-like receptors (NLRs) and RIG-like receptors (RLRs). PRR activation can lead to a cascade of signalling transduction and upregulation of a variety of inflammatory gene expression. The primary role of microglial activation is to eliminate the insults (e.g., dead cells or invading pathogens), which therefore is neuroprotective (4, 5). Under certain conditions, active microglia can promote neuronal regeneration (6). Uncontrolled microglial activation, however, is detrimental and contributes to various neurodegenerative diseases such as Alzheimer's disease (7, 8), Parkinson's disease (9), age-related macular degeneration (AMD) (10–12), diabetic retinopathy (13, 14), inherited retinal degeneration (15) and glaucoma (16). Targeting microglial activation is considered to be an effective approach for the management of neurodegenerative diseases (17–19). Until now, the attempts to control microglial activation with general immune suppression (steroids or immune suppressive drugs) have achieved limited clinical success (20–22). In most conditions, microglial activation is secondary to other pathological processes that damage the CNS or retina. Thus, activated microglia may both exacerbate pathology and aid tissue repair. To develop effective microglia-targeted therapy, it is important that we understand the molecular pathways specific to the neurotoxic effects of activated microglia.

Microglial activation is tightly controlled at multiple levels. Microglia express various receptors (e.g., CX3CR1, SIRPα and CD200R) that can sense inhibitory molecules from surrounding neurons (e.g., CX3CL1, CD47 and CD200 from ganglion cells and amacrine cells of the retina) (23–25). This neuron-to-microglia communication prevents overt microglial activation and protects neurons (23, 24). For example, when the CX3CL1-CX3CR1 pathway is disrupted, microglial activation and retinal degeneration is increased in diabetes (26) or acute stress conditions (27). Microglial activation is also regulated at intracellular levels. When the PRRs or cytokine receptors of microglia are activated, the intracellular signalling transduction pathways are regulated by various immune checkpoint proteins. The Janus kinase (JAK) and signal transducer and activator of transcription protein (STAT) signalling pathway of the cytokine receptors are negatively regulated by the suppressor of cytokine signaling (SOCS) proteins (28, 29). Studies have shown that deletion of *Socs3* in LysM^{+} cells (*LysMCre-Socs3*$^{fl/fl}$) did not affect microglia in normal conditions, yet enhanced the inflammatory response in the CNS in experimental autoimmune encephalomyelitis and increased demyelination (30). The inflammatory response in experimental autoimmune uveoretinitis was also exaggerated in *LysMCre-Socs3*$^{fl/fl}$ mice accompanied by severe retinal degeneration and angiogenesis (31). The *LysMCre-Socs3*$^{fl/fl}$ mice also developed more severe diabetic retinopathy compared with WT mice (32). These results suggest that SOCS3 and CX3CR1 are both critically involved in regulating microglial activation in disease conditions.

During aging, oxidative stress accumulates in the retina, particularly the macula. As a result, a low-grade parainflammation, presented as mild microglial activation, subretinal migration and complement activation is initiated (33). This parainflammatory response, when controlled properly, is beneficial and the retina may age healthily. When the parainflammatory response is dysregulated, it may turn into chronic inflammation leading to retinal degeneration (11). We hypothesized that the combined deletion of two negative immune regulators in microglia, CX3CR1 in the cell surface and SOCS3 in the cytosol, may subject the cells to uncontrolled activation in response to age-mediated low-levels of oxidative insults. In this study, we generated a *Cx3cr1* and *Socs3* double knockout (*LysMCre-Socs3*$^{fl/fl}$*Cx3cr1*$^{gfp/gfp}$) mouse line (referred to as DKO mice in this paper), in which *Cx3cr1* was deleted globally and *Socs3* was deleted in LysM^{+} cells using the Cre/LoxP technology (Additional file 1B). In the retina, these two genes were depleted only in innate immune cells, predominately microglia. We found that the DKO mice presented with significant microglial dysfunction, and with ageing, microglia were activated accompanied by substantial neuronal degeneration – a typical example of primary microglial disorder-mediated pathology i.e., “microgliopathy” (34).

Materials And Methods

- Animals and study design

C57BL/6J wild type, *Socs3*$^{fl/fl}$ (31), *LysMCre-Socs3*$^{fl/fl}$ (31), *Cx3cr1*$^{gfp/gfp}$ (27, 35) and *LysMCre-Socs3*$^{fl/fl}$*Cx3cr1*$^{gfp/gfp}$ DKO mice (all in C57BL/6J background) were used in the study. The *Socs3*$^{fl/fl}$ mice served as WT control. The *LysMCre-Socs3*$^{fl/fl}$ mice were obtained by crossbreeding *Socs3*$^{fl/fl}$ mice with *LysMCre* mice (31). The *Cx3cr1*$^{gfp/gfp}$ mice were provided by Steffen Jung (Weizmann Institute of Science, Rehovot, Israel). The *LysMCre-Socs3*$^{fl/fl}$ mice and *Cx3cr1*$^{gfp/gfp}$ mice were used to generate heterozygous *LysMCre*$^{+/-}$*Socs3*$^{fl/-}$*Cx3cr1*$^{+/gfp}$ mice. Subsequent crossings between offspring mice allowed the generation of *LysMCre-Socs3*$^{fl/fl}$*Cx3cr1*$^{gfp/gfp}$ DKO (Abbreviated as DKO in the following context) mice (Additional file 1). The genotype of the DKO mice was confirmed by PCR (Additional file 1C). Mouse strains used for this study were listed in additional file 2. All animal procedures were conducted in accordance with the Animals (Scientific Procedures) Act of the UK Home Office (1986) and were approved by the Animal Welfare and Ethics Review Body of Queen's University Belfast. All mice were housed at the Biological Research Unit at Queen's University Belfast in a 12-hrs light / dark cycle with free access to water and food.

- Fundus photography and Micron IV examination

Fundus images were obtained. Animals were anesthetized with an intraperitoneal injection of 60 mg/kg ketamine hydrochloride (Fort George Animal Centre, Southampton, UK) and 5 mg/kg xylazine (Pharmacia & Veterinary Products, Kiel, Germany). The pupils were dilated with a drop of tropicamide and phenylephrine (Chauvin, Essex, UK). Images were captured with a Nikon D90 camera via an endoscope (36, 37) or the Micron IV system (Phoenix Research Labs, Pleasanton, CA, USA). Retinal green fluorescent

images in *Cx3cr1*$^{gfp/gfp}$ and DKO mice were acquired using the Micron IV system. The illumination settings and the gain were consistent in each subject. Images were saved in TIFF format.

- Retinal and RPE/Choroidal flatmount preparation and staining

The eyes were collected and fixed with 2% paraformaldehyde (PFA, Agar Scientific Ltd. Cambridge, UK) for 2 h at room temperature. The anterior segment (cornea, iris and ciliary body, and lens) of the eye was removed. Retinal tissue was carefully removed from the eyecup. Retinal tissues and RPE/choroid/sclera eye-cups were processed for flatmount staining using the protocol described in our previous paper (38, 39). The antibodies used in the study were detailed in Table 1. All samples were examined by Dmi8 fluorescence microscopy (Leica Microsystems CMS, Mannheim, Germany). Images were analysed using ImageJ (National Institutes of Health, Bethesda, MD, USA).

Table 1
Antibodies and binding protein/peptide

	Name	Dilution	Company	Host/Type
Antigen	IBA-1	1:200	Wako	Rabbit
	Cone arrestin	1:1000	Chemicon	Rabbit
	PKCα	1:500	Santa Cruz	Rabbit
	Secretagogin	1:500	Biovendor R&D	Sheep
	GFAP	1:250	Abcam	Rabbit
Protein/peptide	Isolectin B4	1:200	Vector	
	Alexa Fluor™ 594 Phalloidin	1:100	ThermoFisher	
Secondary Ab	Alexa Fluor 594	1:400	Invitrogen	Donkey anti-rabbit
	Alexa Fluor 488	1:400	Invitrogen	Donkey anti-rabbit
	Streptavidin, Alexa Fluor™ 594	1:400	Invitrogen	

H&E staining and immunohistochemistry Eyes were fixed as described above and processed for 6 µm-thick paraffin sections. Eye sections were dewaxed using xylene, dehydrated by ethanol and rehydrated by H_2O. Sections were then processed for either H&E staining or immunohistochemistry. Antigen retrieval was carried out using 0.05% citraconic anhydride buffer (Sigma-Aldrich, St. Louise, Missouri, USA) in a 95 °C water bath for 30 min. Sections were permeabilized with 0.5% Triton 100X in PBS for 15 min at room temperature and blocked using 5% BSA for 1 h. Sections were then incubated with primary antibodies (Table 1) overnight at 4 °C. After thorough washes, samples were incubated with secondary antibody for 1 h at room temperature. Samples were mounted with Vectashield mounting medium containing DAPI (Vector Laboratories) and examined by fluorescence microscopy (Leica Dmi8).

Quantification of microglial number in retinal and RPE/choroid flatmounts

Z-stack images (20X) with 1μm intervalswere taken from the mid-central part of the retina in each flatmount (4 images/flatmount). Cells in threedifferent layers, i.e., GCL+IPL, OPL, outer nuclear layer + photoreceptor layer (ONL+PRL) of each z-stack image were quantified by Fiji software (National Institutes of Health, Bethesda, MD). The numbers were normalized to per mm^2 retinal area. For RPE/choroidflatmounts, images were obtained for the entire tissue and the total number of microglia was manually counted.

Quantification of retinal neurons

Fluorescent images were obtained to quantify the number of individual retinal neurons and neuronal structure. Three sections around the optic disc were used for retinal neuronal investigations, with 3-5 eyes used in each group. Four images were taken from the mid-central part of the retina in each eye section. The settings of fluorescence microscope remained constant between images and images were analyzed using FIJI software (National Institutes of Health, Bethesda, MD). The following retinal cells were quantified and analysed using the methods established in our groups(40, 64): 1) Rod and cone photoreceptor (cone arrestin$^+$) cell count ; 2) Cone photoreceptor segment length ; 3) Cone-bipolar (PKCα$^+$) cell number; 4) Rod-bipolar (secretagogin$^+$) cell number; and 5) GABA$^+$amacrine cell number. Cell numbers were averaged and normalised.The quantificationwas confirmed by two independentresearchers.

Quantification of microglial cells and RPE morphology in aged DKO RPE/Choroid flatmounts

Five fluorescent images (40X objective lens) were taken from each RPE/choroidal flatmount. The number of microglial cells and the morphology of RPE in aged DKO mice were quantified. 6 eyes per group were used in this study. FIJI ImageJplug-in Bio-voxxel software (41) was used to outline the shape of each RPE cell. For each RPE cell, the area and perimeter were measured using FIJI and the shape factorwas calculated by the equation $4\pi * Area/Perimeter^2$(42).The shape factor value ranges from 0 to 1, with one indicating a perfect circular cell, and zero indicating an elongated cell. The shape factor of a perfect hexagonal cell (eg. an RPE cell) is around 0.9 (43).The relationship between microglial cell number and the shape factor of the RPE was analyzed by linear regression using SPSS statistics software (IBM, Chicago, IL, USA).The quantification was confirmed by two independentresearchers.

Primary microglial cell culture and treatments

Microglia were cultured from 4-6 week old *Socs3$^{fl/fl}$*and DKO mice using a previously described protocol(44). Briefly, smashed brain tissue suspensions were filtered through a 70 μm cell strainer (BD

Falcon, BD Biosciences). Then the cell suspensions were centrifuged at 600g for 8 min. The cell pellet was re-suspended in media containing 10% fetal calf serum (FCS), 20ng/ml M-CSF (Bio-techne, Minneapolis, Minnesota,US), 1% penicillin/streptomycin, 1 mM glutamine in DMEM/F12 (all from Thermo Fisher Scientific, Waltham, MA, USA), and seeded in a 6-well plate (Thermo Fisher Scientific). Floating cells were removed 3 days later and media were changed every 3 days until cells reached 90% confluence. The phenotype of the cells was confirmed by their CD11b and IBA-1 expression (>90%).The microglia were then treated with 1) M1, or pro-inflammatory stimuli by adding 100ng/ml IFN-γ (Bio-Techne)and 50ng/ml LPS (Sigma-Aldrich)or 2) M2, or anti-inflammatory stimuli by adding 20ng/ml IL-4 (Bio-Techne) overnight. The cells were collected for real-time RT-PCR for cytokine/chemokine gene expression and the supernatants were collected for Luminex assay.

Phagocytosis assay

Microglia from *Socs3*$^{fl/fl}$or DKO mice were seeded into a 96-well plate at the density of 1×10^5/well. The phagocytosis assay was performed using 1) the pHrodo™ Red *E. coli*BioParticles™ and2) *Escherichia coli* (K-12 strain) Alexa Fluor 594 BioParticles™ (both from Thermo Fisher Scientific)following the manufacturer's instructions. For pHrodoRed *E.coli*, fluorescence intensity was measured at 0.5h, 1h, 2hand 3h after incubation using Fluostar Omega microplate reader (BMG Labtech, Ortenberg, Germany) with 550 nm excitation wavelength and a 600 nm emission filter. Bioparticles alone without cells acted as a background control. Phagocytosis was calculated by subtracting the average fluorescence intensity of the background control wells from the experimental wells. Alexa Fluor 594 conjugated *E.coli* was washed with PBS after 0.5h incubation, and fluorescence intensity was measured with the same wavelength. Representative images were taken using the Leica DMi8 microscope.

Reverse transcription and real-time RT-PCR

Total RNA was extracted from retinal tissues by RNeasy Mini kit (Qiagen Ltd, Crawley, UK) according to the manufacturer's instructions. The quantity and quality of RNA were determined using a NanoDrop ND-1000 spectrophotometer (NanoDropTechnologies, Wilmington, DE). The same amount of RNA wasapplied for reverse transcription using SuperScrip™ II Reverse Transcriptase kit and random primers (Invitrogen). Real-time RT-PCR was performed using SYBR Green Master (Roche Diagnostics GmbH, Mannheim, Germany) in the LightCycler® 480 system (Roche Diagnostics GmbH). The primer sequences are listed in Table 2. β-actin was used ashousekeeping control.

Table 2. Primers and their sequences for real time RT-PCR

Genes	Forward	Reverse
βactin	GGCACCACACCTTCTACAATG	GGGGTGTTGAAGGTCTCAAAC
TNFα	TCTCATGCACCACCATCAAGGACT	ACCACTCTCCCTTTGCAGAACTCA
iNOS	TCTTTGACGCTCGGAACTGTAGCA	ACCTGATGTTGCCATTGTTGGTGG
IL-1β	AAGGGCTGCTTCCAAACCTTTGAC	ATACTGCCTGCCTGAAGCTCTTGT
IL-6	ATCCAGTTGCCTTCTTGGGACTGA	TAAGCCTCCGACTTGTGAAGTGGT
IL10	GGCAGAGAACCATGGCCCAGAA	AATCGATGACAGCGCCTCAGCC
IL12p40	ATGGCCATGTGGGAGCTGGAGAAAG	GTGGAGCAGCAGATGTGAGTGGCT
IL23p19	ATGTGCCCCGTATCCAGTGT	GGGGTGATCCTCTGGCTGGA
ARG1	TTATCGAGCGCCTTTCTCAA	TGGTCTCTCAGGTCATACTCTGT
CD206	TCAGCTATTGGACGCGAGGCA	TCCGGGTTGCAAGTTGCCGT
CCL2	GCATCCACGTGTTGGCTCA	CTCCAGCCTACTCATTGGGATCA
CCL5	ACTCCCTGCTGCTTTGCCTAC	GAGGTTCCTTCGAGTGACA
CXCL2	AAGTTTGCCTTGACCCTGAA	AGGCACATCAGGTACGATCC

Luminexmultiplex assay

The cytokine & chemokine magnetic bead panel kit (LXSAMSM-10, R&D, USA) was designed to detect CCL2, CCL5, CXCL2, CXCL10, Granulocyte-macrophage colony-stimulating factor (GM-CSF), IL-1β, IL-6, IL-10, IL-12p70 and TNF-α in the supernatant after different treatments. All procedures were carried out according to the manufacturer's instructions. The signals were detected and data analyzed by the Bio-plex 200 System (BIO-RAD, Richmond, CA). Chemokine concentrations were calculated using StarStation software (Applied Cytometry Systems, UK) with a four parameter curve-fitting algorithm applied for standard curve calculation.

Retinal explants and microglia co-culture

The method for retinal explants and microglia co-culture was adapted from a previously published paper (45). Briefly, microglial cells from *Socs3*$^{fl/fl}$and DKO mice were seeded onto polycarbonate filters (Fisher scientific, UK) and cultured inDMEM/F12 for 24h to allow firm attachment to the filters. Cells were then given M0/ M1/ M2 treatments for overnight. Cells were washed with PBS three times to remove stimuli. Retinas from C57BL/6J mice were placed with the photoreceptor sidein contact with microglia for 24h at 37˚C. Retinal explants were fixed and stained for cone arrestin.

Statistical analysis

Statistical analysis was performed inGraphPad Prism (GraphPad Software, San Diego, CA, USA) and SPSS. Student's t tests were performed for analysis and comparisons between two groups. Two-way analysis of variance (ANOVA) followed by Sidak'sor Tukey multiple comparison test were used to investigate the difference between groups as indicated in individual figure legends. Data are presented as mean ± SD and significance was established as $P < 0.05$.

Results

- General phenotype of the DKO mice

The DKO mice bred normally and litter size was similar to C57BL/6 WT and *Socs3*$^{fl/fl}$ control mice. They were not were prone to infections in our Specific Pathogen-Free (SPF) standard housing facility. Some mice started showing signs of slower and limited movements at 7 ~ 8 months old. 57% of the DKO mice died before 12 months old and the majority of deaths occurred between 7–9 months of age (Additional file 3). Post-mortem investigations (n = 27 mice) showed that ~ 30% of the mice had tumors in the liver, spleen, and intestinal system. No visible abnormality was observed in the brain, the lung or the heart. The majority of the DKO mice died before 15 months of age. Our results suggest that the DKO mice may have accelerated aging.

- Retinal microglial activation in DKO mice

As the two immune regulatory genes, *Cx3cr1* and *Socs3*, were depleted exclusively in microglia in the retina, we examined microglial cells under normal aging conditions. For this purpose, we compared the DKO mice with each single KO mice (*Cx3cr1*$^{gfp/gfp}$ and *LysMCre-Socs3*$^{fl/fl}$) and used the *Socs3*$^{fl/fl}$ mice as WT controls. Due to the short lifespan of the DKO mice, "aged" mice were 10–12 months old and "young" mice were 3–5 months old in this study.

Retinal microglia in the *Cx3cr1*$^{gfp/gfp}$ and DKO mice were imaged *in vivo* due to their GFP expression. Fundus images did not show any abnormality in 3 and 12 month-old *Cx3cr1*$^{gfp/gfp}$ mice and 3 month-old DKO mice (Figs. 1A-C). Patches of whitish lesions and multiple small whitish dots were observed in 75% of 12 month-old DKO mice (arrow and arrowheads, Fig. 1D). These lesions were not observed in age-matched *LysMCre-Socs3*$^{fl/fl}$ and *Socs3*$^{fl/fl}$ mice (Data not shown). Dense GFP signals were observed in the optic disc (OD) in *Cx3cr1*$^{gfp/gfp}$ and DKO mice (Figs. 1E-H). GFP^{+} microglia were evenly distributed throughout the fundus. Perivascular macrophages were also visible in some areas (Fig. 1E-G, arrowhead). No obvious difference was observed between 3 month old *Cx3cr1*$^{gfp/gfp}$ and DKO mice. The density of GFP^{+} cells appeared to be increased in 12 month old DKO mice and patches of GFP aggregations were observed in these mice (Fig. 1H, arrows).

Microglia were further quantified in retinal flatmounts in all groups. Microglia in *Socs3*$^{fl/fl}$ and *LysMCre-Socs3*$^{fl/fl}$ mice (which do not express GFP) were identified by IBA-1 staining. In 3 month old mice, IBA-1^{+} cells resided in the GCL and IPL (Fig. 2A, D), and OPL (Fig. 2B, E). The numbers of microglia in the GCL and IPL were comparable in all four groups; whereas DKO mice had higher number of microglia in the OPL than those in other strains (Fig. 2E). In the aged mice, in addition to GCL, IPL and OPL, microglia were detectable in the outer retinal layers, including ONL + PRL, particularly in DKO mice (Fig. 2C, F). Aged DKO mice had a significantly higher number of microglia than other age-matched strains in all layers studied (Fig. 2G). The number of microglia in RPE flatmounts of aged DKO mice were significantly higher than those in other age-matched strains (Additional file 4A, B). Microglia in photoreceptor layer and RPE flatmounts of aged DKO mice also expressed Isolectin B4, indicative of microglial activation (Additional file 4C). Our results suggest that age-related microglial activation was significantly enhanced in the DKO mice compared with *Socs3*$^{fl/fl}$ and single KO mice.

- Retinal neuronal degeneration in aged DKO mice

To understand if uncontrolled microglial activation led to retinal pathology in the DKO mice, immunohistological investigations on retinal neurons were conducted. In young mice, with the exception of a slightly decreased number of cone photoreceptors in DKO mice, the numbers of cells in the entire ONL, cone arrestin^{+} photoprecetors, and rod photoreceptors were comparable in different strains of mice (Fig. 3A-E). In aged mice, the numbers of cells in the ONL, cone arrestin^{+} photoreceptors and rod photoreceptors were significantly decreased in DKO mice compared with single KO and *Socs3*$^{fl/fl}$ mice (Fig. 3A-E), accompanied by reduction of the length of cone photoreceptor segments (Fig. 3F-G).

The number of secretagogin^{+} rod-bipolar cells was lower in young DKO mice than age-matched single KO or *Socs3*$^{fl/fl}$ controls and was further reduced in aged DKO mice (Fig. 4A-B). The number of PKCα^{+} cone-bipolar cells was comparable in young mice (Fig. 4C-D). An age-related reduction was observed in *Cx3cr1*$^{gfp/gfp}$ and DKO mice although the reduction was more significant in aged DKO mice (Fig. 4C-D). The number of GABAergic^{+} cells (including GABA^{+} amacrine cells in the INL and displaced amacrine cells in the GCL) was significantly lower in young DKO mice (Fig. 4E-F). The age-related reduction was observed in all strains of mice although the reduction was more profound in DKO mice (Fig. 4E-F).

Histological investigation did not show any structural abnormalities in eyes from young mice (Fig. 5A). Localized RPE swelling (Fig. 5A, arrows) and vacuoles (Fig. 5A, asterisks) with thinner ONL in corresponding area were frequently observed in aged DKO mice. RPE damage in aged DKO mice was further confirmed in flatmount investigations and the lesions were always accompanied by microglial/macrophage infiltration (Fig. 5B). Aged DKO mice had enlarged RPE cell size, increased perimeter and reduced cell density. Areas of total RPE damage with massive microglial infiltration were frequently observed in aged DKO mice (Fig. 5B). The number of infiltrating microglia/macrophages negatively correlated with RPE shape factor in aged DKO (Fig. 5C).

In line with retinal neuronal degeneration, we also observed increased GFAP expression in 10 ~ 12 month old DKO mice (Additional file 5), indicative of Müller gliosis.

Our results suggest that aged DKO mice suffered from significant neuroretinal degeneration and RPE damage.

- Enhanced phagocytic activity in microglia from DKO mice
- To understand how *Cx3cr1* and *Socs3* depletion may affect microglial function, microglial cultures from the DKO and *Socs3*$^{fl/fl}$ mice were subjected to phagocytosis assay using the Alexa Fluor™ 594 conjugate E. coli BioParticles™ and the pH-sensitive pHrodo™ Red E. coli BioParticles™ systems. In both assays, microglia from DKO mice had significantly higher levels of fluorescence intensities compared to cells from control mice (Fig. 6A-C). Fluorescence microscopy showed intense intracellular particles in DKO cells treated with Alexa Fluor™ 594 E. coli bioparticles (although un-ingested extracellular bioparticles were also visible) (Fig. 6B). In cells treated with pH-sensitive bioparticles, fluorescent signals were inside the cells and DKO cells demonstrated brighter fluorescent signals than *Socs3*$^{fl/fl}$ cells (Fig. 6C). Our results suggest that the phagocytic activity of DKO microglia was significantly higher than that of *Socs3*$^{fl/fl}$ cells. Interestingly, we also detected cone arrestin antigens inside GFP^{+} cells in retinal sections from aged DKO mice but not in other strains (Fig. 6D), an indication of *in situ* uptake of damaged cone photoreceptors by microglia.
- Altered cytokine expression and secretion by microglia from DKO mice

Under normal culture conditions, naïve microglia (M0) from DKO mice expressed significantly higher levels of TNFα and iNOS mRNA (Fig. 7A) and produced significantly higher amounts of TNF-α, IL-6, CCL2, CCL5, CXCL2 and CXCL10 proteins compared to their counterparts from *Socs3*$^{fl/fl}$ mice (Fig. 7B).

Following LPS + IFN-γ stimulation (M1), increased mRNA expressions of pro-inflammatory mediators such as TNF-α, iNOS, IL-1β, IL-6, IL-12p40, IL-23p19, CCL2, CCL5 and CXCL2 were observed in microglia from both *Socs3*$^{fl/fl}$ and DKO mice compared to naïve M0 cells although the upregulations were generally more significant in DKO M1 cells compared to *Socs3*$^{fl/fl}$ M1 cells (Fig. 7A). M1 microglia from DKO mice produced and released significantly higher levels of TNF-α, IL-6, CCL2, CCL5, CXCL2, CXCL10 and IL10 compared with M1 microglia from WT mice (Fig. 7B). Interestingly, although the mRNA of IL-1β was significantly increased in M1 microglia, this cytokine was below detectable levels in the supernatants (data not shown).

IL-4 treated microglia (M2) from DKO mice expressed significantly higher levels of IL10, CD206 and Arg1 mRNA compared to their counterpart from *Socs3*$^{fl/fl}$ mice (Fig. 7A). Interestingly, the productions of TNFα, IL-6, CCL2, CCL5, CXCL2 and CXCL10 were also significantly higher in IL4-treated DKO microglia than those in IL4-treated *Socs3*$^{fl/fl}$ microglia (Fig. 7B).

Together, our data suggested that microglia with *Socs3* and *Cx3cr1* deficiency produce significantly higher basal levels of cytokines and chemokines, and they are also more sensitive to cytokine stimuli (such as LPS + IFNγ or IL-4).

- Microglia induced photoreceptor death in retinal explants

To further understand if altered microglial activation contributes to retinal degeneration in aged DKO mice, retinal explants from C57BL/6J WT mice were cultured alone or co-cultured with microglia from *Socs3*$^{fl/fl}$ and DKO mice without and with M1 or M2 polarization (Fig. 8A), and the number of cone arrestin^{+} cells was evaluated in retinal flatmounts. The addition of naïve (M0) microglia from *Socs3*$^{fl/fl}$ or DKO mice did not affect the number of cone arrestin^{+} cells compared to retinal explants alone (109.14% and 100.42% respectively, Fig. 8B, C). M1-type microglia from both *Socs3*$^{fl/fl}$ and DKO significantly reduced cone photoreceptor survival (73.67% and 64.87% respectively, Fig. 8B, C). Interestingly, M2-type microglia from DKO but not *Socs3*$^{fl/fl}$ mice also significantly reduced cone photoreceptor survival (57.48%, Fig. 8B, C). Our results suggest that active microglia from DKO mice are toxic to photoreceptors regardless of how they are activated; whereas, microglia from *Socs3*$^{fl/fl}$ mice are only toxic to photoreceptors when they are activated to a pro-inflammatory phenotype.

Discussion

In this study, we showed that deletion of two immune negative regulators, *Cx3cr1* and *Socs3* (in LysM^{+} cells) resulted in uncontrolled retinal microglial activation during aging, accompanied by a significant degeneration of retinal neurons and RPE cells. Although *Cx3cr1* was deleted globally, it is expressed exclusively by microglia and perivascular macrophages in the retina. *Lysozyme 2* (*LysM* or *Lyz2*) is expressed by all retinal microglia and macrophages and by a small population (< 8%) of ganglion cells and amacrine cells (46). Deletion of *Cx3cr1* and *Socs3* in the DKO mice would therefore predominately affect retinal microglia. The degeneration of retinal neurons in the aged DKO mice was likely the consequence of primary microglial dysfunction. Therefore, retinal pathologies observed in this study fall into the disease category of “microgliopathay” (47).

The DKO mice were not prone to any infection when housed in a standard SPF facility although the lifespan of the DKO mice was significantly shortened compared to WT or single KO mice. The DKO mice appeared to have slower and limited movements and higher incident of tumor development (evidence of accumulation of mutations). This suggests that the DKO mice might have accelerated aging. Therefore, this mouse model may be valuable for understanding the contribution of low-grade chronic inflammation (inflammaging) (48) to the aging process.

Retinal aging is accompanied by a low-grade of parainflammation characterized by mild microglial activation, subretinal migration and complement activation (33, 49), and a dysregulated parainflammatory response contributes critically to age-related retinal degenerative diseases such as AMD (11). Previous studies have shown that the mice with *Cx3cr1* deficiency developed retinal

degeneration by 1–2 years of age (50, 51), and the pathology is known to be related to increased subretinal infiltration of $CCR2^{+}$ phagocytes and the impairment in their removal (51). In our study, significant microglial activation and retinal degeneration were only observed in DKO mice by the age of 10–12 months. Our results suggest that microglial activation is collectively regulated by neuron-derived signals (e.g., CX3CL1) and intracellular immune inhibitors (e.g., SOCS3). The discrepancy in retinal pathology in *Cx3cr1* KO mice between our study and that of Combadiere *et al.* may be related to different housing conditions.

We observed a number of functional alterations in microglia from the DKO mice. These include higher cytotoxicity to photoreceptors in retinal explants, significantly higher levels of phagocytic activities and more secretory proteins (TNFα, IL6, CCL2 CCL5, CXCL2, CXCL10 and IL10). The secretory profile was similar to the senescence-associated secretory phenotype (SASP) of macrophages (52) with the exception of IL1β, which was not detected in microglial supernatants in our study. The JAK/STAT pathway is known to be involved in cell senescence and the phenotype of SASP (53) and JAK inhibition alleviated SASP phenotype and frailty in old age (53). Previously, we have shown that the *LysMCre-Socs3*$^{fl/fl}$ mice had higher levels of pSTAT3 in the retina (54). Furthermore, a recent study has shown that CX3CR1-deficient microglia exhibit a premature aging transcriptome (55). It is possible that microglia from the DKO mice may also undergo premature aging although this warrants further investigation.

SASP can have significant pathological effects on the aging retina. In our study, microglia from DKO mice produced significantly higher levels of cytokines and chemokines compared to their counterparts regardless of their activation states (Fig. 7B); however, only M1 and M2 (but not naïve M0) microglia were toxic to photoreceptors in retinal explants (Fig. 8B-C). Compared to naïve (M0) microglia, M2 microglia from DKO mice produced higher levels of IL6, CCL2 and CXCL2, suggesting that the three mediators might contribute to M2 microglia-mediated photoreceptor death.

A recent study has shown that microglial function is distinct in different anatomical locations during retinal homeostasis and degeneration (56). We have shown that microglia in different retinal layers are regulated by diverse neurons and molecules (25). Specifically, ganglion cell and amacrine cells work together to control microglial activation in the GCL/IPL layer; whereas microglia in the OPL is regulated by horizontal cells and photoreceptors assisted by bipolar cells (25). In the present model of retinal microgliopathy, microglia in all retinal layers were activated and a wide range of retinal neurons and RPE cells were affected. The initial trigger of retinal microglial activation in the aging DKO mice would likely be oxidative stress. Previously, we detected ox-LDL and 2,4-Dinitrophenol (DNP) in all retinal layers of the aged mice (33) suggesting ubiquitous oxidative stress in the aging retina. Our results also suggest that that Cx3cr1 and Socs3 are involved in the parainflammatory response of microglia in all retinal layers.

The crosstalk between microglia and retinal neurons is important for maintaining retinal homeostasis. Active microglia release excessive amounts of proinflammatory cytokines and chemokines that kill retinal neurons. Dead neurons in turn, further stimulate microglial activation. The reduction in retinal neurons also weakens the inhibitory signals to microglia further escalating microglial activation. Apart from

expressing the SASP, microglia in the DKO mice also had enhanced phagocytic activities and the hyperactive engulfment (named as phagoptosis by (57)) can also lead to unnecessary neuron loss (58). Recent evidence indicates that phagoptosis contributes to neuronal loss in various CNS diseases (59–61).

The damage to RPE cells in our model may be a consequence of excessive retinal neuronal degeneration. We observed a strong correlation between the number of subretinal microglia/macrophage and RPE dysmorphology (Fig. 6B-C). Damaged neurons are removed from the retina by subretinal phagocytes (including microglia), likely through the subretinal space – RPE – choroid route (a CD47-dependent pathway) (62). Impaired elimination ability of these subretinal phagocytes is known to contribute to RPE damage and the development of age-related macular degeneration (63). Although we do not know if the mechanisms involved in subretinal phagocyte elimination is altered in the DKO mice, the continued retinal neuronal damage during aging may lead to accumulation of active phagocytes into the subretinal space, which may cause RPE damage (63).

Conclusions

Age-induced retinal microglial activation in the *LysMCre-Socs3*$^{fl/fl}$*Cx3cr1*$^{gfp/gfp}$ *D*KO mice is dysregulated. This uncontrolled low-grade microglial activation resulted in retinal microgliopathy characterized as extensive neuronal degeneration and RPE damage. In this model of microgliopathy, active microglia may damage neurons through SASP expression or phagoptosis although the underlying mechanisms remain to be investigated. This model offers a unique opportunity to study the mechanisms of microglial dysfunction-mediated retinal pathology and will also help to elucidate the detrimental role of inflammaging in age-related retinal degeneration.

List Of Abbreviations

AMD	Age-related macular degeneration
Arg1	Arginase 1
CCL	C-C Motif Chemokine Ligand
CD	Cluster of differentiation
CNS	Central nervous system
CXCL	Chemokine (C-X-C motiv) ligand
DAMPs	Damage-associated molecular patterns
DKO	Double knock-out
GCL	Ganglion cell layer
GFP	Green fluorescent protein
IB4	The α-d-galactosyl-specific isolectin B
IBA-1	Ionized calcium binding adaptor molecule 1
IFN-γ	Interferon gamma
IL	Interleukin
IPL	Inner plexiform layer
JAKs	Janus kinases
KO	Knock-out
LPS	Lipopolysaccharide
NLRs	NOD-like receptors
ONL	Outer nuclear layer
OPL	Outer plexiform layer
PAMPs	Pathogen-associated molecular patterns
PRL	Photoreceptor layer
PRRs	Pattern recognition receptors
RLRs	RIG-like receptors
RPE	Retinal pigment epithelium
RT-PCR	Real time-polymerase chain reaction
Socs3	Suppressor of cytokine signaling 3
STATs	Signal transducer and activator of transcription proteins

TLRs	Toll-like receptors
WT	Wild type

Declarations

Ethics statement

All procedures concerning animals were performed with permission of the local authority.

Conflict of Interest

The authors declare that the research was conducted in the absence of any commercial or financial relationships that could be construed as a potential conflict of interest.

Ethics approval and consent to participate

Not applicable

Consent for publication

Not applicable

Availability of data and materials

All data generated or analysed during this study are included in this published article (and its additional files).

Competing interests

The authors declare that they have no competing interests.

Funding

This work was supported by China Scholarship Council and Fight for Sight (UK) (1361/62).

Author Contributions

XD: Experimental execution, data analysis, writing the manuscript; RP: Experimental execution and data analysis; KL: Data analysis; AK: KO and DKO mouse models generation; MC: Experimental design/Concept, editing the manuscript; HX: Experimental design/Concept, data analysis and interpretation, writing the manuscript. All authors read and approved the final version of the manuscript.

Acknowledgments

The authors thank John Conlon for helping with the Luminex Assay and Daniel Xu for helping with English expression.

References

1. Wheeler DL, Sariol A, Meyerholz DK, Perlman S. Microglia are required for protection against lethal coronavirus encephalitis in mice. J Clin Invest. 2018;128(3):931–43.
2. Zhou LJ, Peng J, Xu YN, Zeng WJ, Zhang J, Wei X, et al. Microglia Are Indispensable for Synaptic Plasticity in the Spinal Dorsal Horn and Chronic Pain. Cell Rep. 2019;27(13):3844–59.e6.
3. Karlstetter M, Langmann T. Microglia in the aging retina. Adv Exp Med Biol. 2014;801:207–12. [cited 2019 Jan 12 ;.
4. Li L, Eter N, Heiduschka P. The microglia in healthy and diseased retina. Exp Eye Res. 2015;136:116–30.
5. Michell-Robinson MA, Touil H, Healy LM, Owen DR, Durafourt BA, Bar-Or A, et al. Roles of microglia in brain development, tissue maintenance and repair. Brain. 2015;138(5):1138–59.
6. Lloyd AF, Davies CL, Holloway RK, Labrak Y, Ireland G, Carradori D, et al. Central nervous system regeneration is driven by microglia necroptosis and repopulation. Nat Neurosci. 2019;22(7):1046–52.
7. Füger P, Hefendehl JK, Veeraraghavalu K, Wendeln AC, Schlosser C, Obermüller U, et al. Microglia turnover with aging and in an Alzheimer's model via long-term in vivo single-cell imaging. Nat Neurosci. 2017;20(10):1371–6.
8. Bachstetter AD, Van Eldik LJ, Schmitt FA, Neltner JH, Ighodaro ET, Webster SJ, et al. Disease-related microglia heterogeneity in the hippocampus of Alzheimer's disease, dementia with Lewy bodies, and hippocampal sclerosis of aging. Acta Neuropathol Commun. 2015 Dec;23(1):32. 3(.
9. Kostuk EW, Cai J, Iacovitti L. Regional microglia are transcriptionally distinct but similarly exacerbate neurodegeneration in a culture model of Parkinson's disease. J Neuroinflammation. 2018;15(1):1–11.
10. Karlstetter M, Scholz R, Rutar M, Wong WT, Provis JM, Langmann T. Retinal microglia: Just bystander or target for therapy? Prog Retin Eye Res. 2015;45:30–57.
11. Chen M, Xu H. Parainflammation, chronic inflammation, and age-related macular degeneration. J Leukoc Biol. 2015 Nov 1;98(5):713–25.
12. Rashid K, Akhtar-Schaefer I, Langmann T. Microglia in Retinal Degeneration. Front Immunol. 2019;10(August):1–19.
13. Zeng HY, Green WR, Tso MOM. Microglial activation in human diabetic retinopathy. Arch Ophthalmol. 2008;126(2):227–32.
14. Omri S, Behar-Cohen F, De Kozak Y, Sennlaub F, Mafra Verissimo L, Jonet L, et al. Microglia/macrophages migrate through retinal epithelium barrier by a transcellular route in diabetic retinopathy: Role of PKCζ in the Goto Kakizaki rat model. Am J Pathol. 2011;179(2):942–53.

15. Gupta N, Brown KE, Milam AH. Activated microglia in human retinitis pigmentosa, late-onset retinal degeneration, and age-related macular degeneration. Exp Eye Res. 2003;76(4):463–71.
16. Bosco A, Romero CO, Breen KT, Chagovetz AA, Steele MR, Ambati BK, et al. Neurodegeneration severity can be predicted from early microglia alterations monitored in vivo in a mouse model of chronic glaucoma. Dis Model Mech. 2015;8(5):443–55.
17. Akhtar-Schäfer I, Wang L, Krohne TU, Xu H, Langmann T. Modulation of three key innate immune pathways for the most common retinal degenerative diseases. EMBO Mol Med. 2018;10:e8259.
18. Du RH, Sun H, Bin, Hu ZL, Lu M, Ding JH, Hu G. Kir6.1/K-ATP channel modulates microglia phenotypes: Implication in Parkinson's disease. Cell Death Dis. 2018;9(3).
19. Lan X, Han X, Li Q, Yang QW, Wang J. Modulators of microglial activation and polarization after intracerebral haemorrhage. Nat Rev Neurol. 2017;13(7):420–33.
20. Nussenblatt RB, Byrnes G, Sen HN, Yeh S, Faia L, Meyerle C, et al. A randomized pilot study of systemic immunosuppression in the treatment of age-related macular degeneration with choroidal neovascularization. Retina. 2010;30(10):1579–87.
21. Rosenberg PB. Clinical aspects of inflammation in Alzheimer's disease. Int Rev Psychiatry. 2005;17(6):503–14.
22. Sandhu HS, Lambert J, Xu Y, Kaplan HJ. Systemic immunosuppression and risk of age-related macular degeneration. PLoS One. 2018;13(9):1–13.
23. Langmann T. Microglia activation in retinal degeneration. J Leukoc Biol. 2007;81(6):1345–51.
24. Chen M, Luo C, Zhao J, Devarajan G, Xu H. Immune regulation in the aging retina. Prog Retin Eye Res. 2019;69(June):159–72.
25. Liu J, Tang M, Harkin K, Du X, Luo C, Chen M, et al. Single-cell RNA sequencing study of retinal immune regulators identified CD47 and CD59a expression in photoreceptors—Implications in subretinal immune regulation. J Neurosci Res. 2020;(October 2019):1498–513.
26. Beli E, Dominguez JM, Hu P, Thinschmidt JS, Caballero S, Li Calzi S, et al. *Cx3cr1* deficiency accelerates the development of retinopathy in a rodent model of type 1 diabetes. J Mol Med. 2016 Nov 25;94(11):1255–65.
27. Chen M, Luo C, Penalva R, Xu H. Paraquat-induced retinal degeneration is exaggerated in *Cx3cr1*-deficient mice and is associated with increased retinal inflammation. Invest Ophthalmol Vis Sci. 2013;54(1):682–90.
28. Yoshimura A, Naka T, Kubo M. SOCS proteins, cytokine signalling and immune regulation. Nat Rev Immunol. 2007;7(6):454–65.
29. Carow B, Rottenberg ME. *Socs3*, a major regulator of infection and inflammation. Front Immunol. 2014;5(Feb):1–13.
30. Qin H, Yeh W, Sarno P, De, Holdbrooks AT, Liu Y, Muldowney MT, et al. Signal transducer and activator of transcription-3/suppressor of cytokine signaling-3 (STAT3/SOCS3) axis in myeloid cells regulates neuroinflammation. Proc Natl Acad Sci U S A. 2012 Mar 27; 109(13): 5004–5009.

31. Chen M, Zhao J, Ali IHA, Marry S, Augustine J, Bhuckory M, et al. Cytokine Signaling Protein 3 Deficiency in Myeloid Cells Promotes Retinal Degeneration and Angiogenesis through Arginase-1 Up-Regulation in Experimental Autoimmune Uveoretinitis. Am J Pathol. 2018 Apr;188(4):1007–20.
32. Chen M, Obasanmi G, Armstrong D, Lavery N, Kissenpfennig A, Lois N. STAT3 activation in circulating myeloid- derived cells contributes to retinal microvascular dysfunction in diabetes. J Neuroinflammation. 2019;16:138.
33. Xu H, Chen M, Forrester JV. Para-inflammation in the aging retina. Prog Retin Eye Res. 2009;28:348–68.
34. Bianchin MM, Martin KC, De Souza AC, De Oliveira MA, De Mello Rieder CR. Nasu-Hakola disease and primary microglial dysfunction. Nat Rev Neurol. 2010;6(9):1–2.
35. Jung S, Aliberti J, Graemmel P, Sunshine MJ, Kreutzberg GW, Sher A, et al. Analysis of Fractalkine Receptor *Cx3cr1* Function by Targeted Deletion and Green Fluorescent Protein Reporter Gene Insertion. Mol Cell Biol. 2000;20(11):4106–14.
36. Xu H, Koch P, Chen M, Lau A, Reid DM, Forrester JV. A clinical grading system for retinal inflammation in the chronic model of experimental autoimmune uveoretinitis using digital fundus images. Exp Eye Res. 2008;87(4):319–26.
37. Paques M, Guyomard JL, Simonutti M, Roux MJ, Picaud S, LeGargasson JF, et al. Panretinal, high-resolution color photography of the mouse fundus. Invest Ophthalmol Vis Sci. 2007;48(6):2769–74.
38. Xu H, Chen M, Manivannan A, Lois N, Forrester JV. Age-dependent accumulation of lipofuscin in perivascular and subretinal microglia in experimental mice. Aging Cell. 2008;7(1):58–68.
39. Xu H, Dawson R, Forrester JV, Liversidge J. Identification of novel dendritic cell populations in normal mouse retina. Invest Ophthalmol Vis Sci. 2007;48(4):1701–10.
40. Hombrebueno JR, Luo C, Guo L, Chen M, Xu H. Intravitreal Injection of Normal Saline Induces Retinal Degeneration in the C57BL/6J Mouse. Transl Vis Sci Technol. 2014;3(2):3.
41. Jan Brocher TW. BioVoxxel Toolbox - ImageJ. 2015 [cited 2018 Dec 15]. Available from: https://imagej.net/BioVoxxel_Toolbox.
42. Versaevel M, Grevesse T, Gabriele S. Spatial coordination between cell and nuclear shape within micropatterned endothelial cells. Nat Commun. 2012;3:617.
43. Chua J, Liew L, Yim E. Cultivation of Human Microvascular Endothelial Cells on Topographical Substrates to Mimic the Human Corneal Endothelium. J Funct Biomater. 2013;4(1):38–58.
44. Wang L, Pavlou S, Du X, Bhuckory M, Xu H, Chen M. Glucose transporter 1 critically controls microglial activation through facilitating glycolysis. Mol Neurodegeneration. 2019;14(1):2.
45. Eandi CM, Messance HC, Augustin S, Dominguez E, Lavalette S, Forster V, et al. Subretinal mononuclear phagocytes induce cone segment loss via IL-1β. Elife. 2016;5(July):1–16.
46. Fouda AY, Xu Z, Narayanan SP, Caldwell RW, Caldwell RB. Utility of LysM-cre and Cdh5-cre Driver Mice in Retinal and Brain Research: An Imaging Study Using tdTomato Reporter Mouse. Invest Ophthalmol Vis Sci. 2020;61(3):51.

47. Prinz M, Priller J. Microglia and brain macrophages in the molecular age: From origin to neuropsychiatric disease. Nat Rev Neurosci. 2014;15(5):300–12.
48. Fulop T, Witkowski JM, Olivieri F, Larbi A. The integration of inflammaging in age-related diseases. Semin Immunol. 2018;Vol. 40:17–35.
49. Chen M, Muckersie E, Forrester JV, Xu H. Immune activation in retinal aging: A gene expression study. Invest Ophthalmol Vis Sci. 2010;51(11):5888–96.
50. Combadière C, Feumi C, Raoul W, Keller N, Rodéro M, Pézard A, et al. *Cx3cr1*-dependent subretinal microglia cell accumulation is associated with cardinal features of age-related macular degeneration. J Clin Invest. 2007;117(10):2920–8.
51. Sennlaub F, Auvynet C, Calippe B, Lavalette S, Poupel L, Hu SJ, et al. CCR2 + monocytes infiltrate atrophic lesions in age-related macular disease and mediate photoreceptor degeneration in experimental subretinal inflammation in *Cx3cr1* deficient mice. EMBO Mol Med. 2013;5(11):1775–93.
52. Wei W, Ji S. Cellular senescence: Molecular mechanisms and pathogenicity. J Cell Physiol. 2018;233(12):9121–35.
53. Xu M, Tchkonia T, Ding H, Ogrodnik M, Lubbers ER, Pirtskhalava T, et al. JAK inhibition alleviates the cellular senescence-associated secretory phenotype and frailty in old age. Proc Natl Acad Sci U S A. 2015;112(46):E6301–10.
54. Chen M, Lechner J, Zhao J, Toth L, Hogg R, Silvestri G, et al. STAT3 Activation in Circulating Monocytes Contributes to Neovascular Age-Related Macular Degeneration. Curr Mol Med. 2016;16(4):412–23.
55. Gyoneva S, Hosur R, Gosselin D, Zhang B, Ouyang Z, Cotleur AC, et al. *Cx3cr1*-deficient microglia exhibit a premature aging transcriptome. Life Sci Alliance. 2019;2(6):1–16.
56. O'Koren EG, Yu C, Klingeborn M, Wong AYW, Prigge CL, Mathew R, et al. Microglial Function Is Distinct in Different Anatomical Locations during Retinal Homeostasis and Degeneration. Immunity. 2019;50(3):723–37.e7.
57. Brown GC, Neher JJ. Eaten alive! Cell death by primary phagocytosis: "Phagoptosis.". Trends Biochem Sci. 2012;37(8):325–32.
58. Brown GC, Neher JJ. Microglial phagocytosis of live neurons. Nat Rev Neurosci. 2014;15(4):209–16.
59. Zhao L, Zabel MK, Wang X, Ma W, Shah P, Fariss RN, et al. Microglial phagocytosis of living photoreceptors contributes to inherited retinal degeneration. EMBO Mol Med. 2015;7(9):1179–97.
60. Hornik TC, Vilalta A, Brown GC. Activated microglia cause reversible apoptosis of pheochromocytoma cells, inducing their cell death by phagocytosis. J Cell Sci. 2016;129(1):65–79.
61. Brelstaff J, Tolkovsky AM, Ghetti B, Goedert M, Spillantini MG. Living Neurons with Tau Filaments Aberrantly Expose Phosphatidylserine and Are Phagocytosed by Microglia. Cell Rep. 2018;24(8):1939–48.e4.

62. Calippe B, Augustin S, Beguier F, Charles-Messance H, Poupel L, Conart JB, et al. Complement Factor H Inhibits CD47-Mediated Resolution of Inflammation. Immunity. 2017;46(2):261–72.
63. Guillonneau X, Eandi CM, Paques M, Sahel JA, Sapieha P, Sennlaub F. On phagocytes and macular degeneration. Prog Retin Eye Res. 2017;61:98–128.
64. Augustine J, Pavlou S, Ali I, Harkin K, Ozaki E, Campbell M, Stitt AW, Xu H, Chen M. IL-33 deficiency causes persistent inflammation and severe neurodegeneration in retinal detachment. J Neuroinflammation. 2019;16:251.

Figures

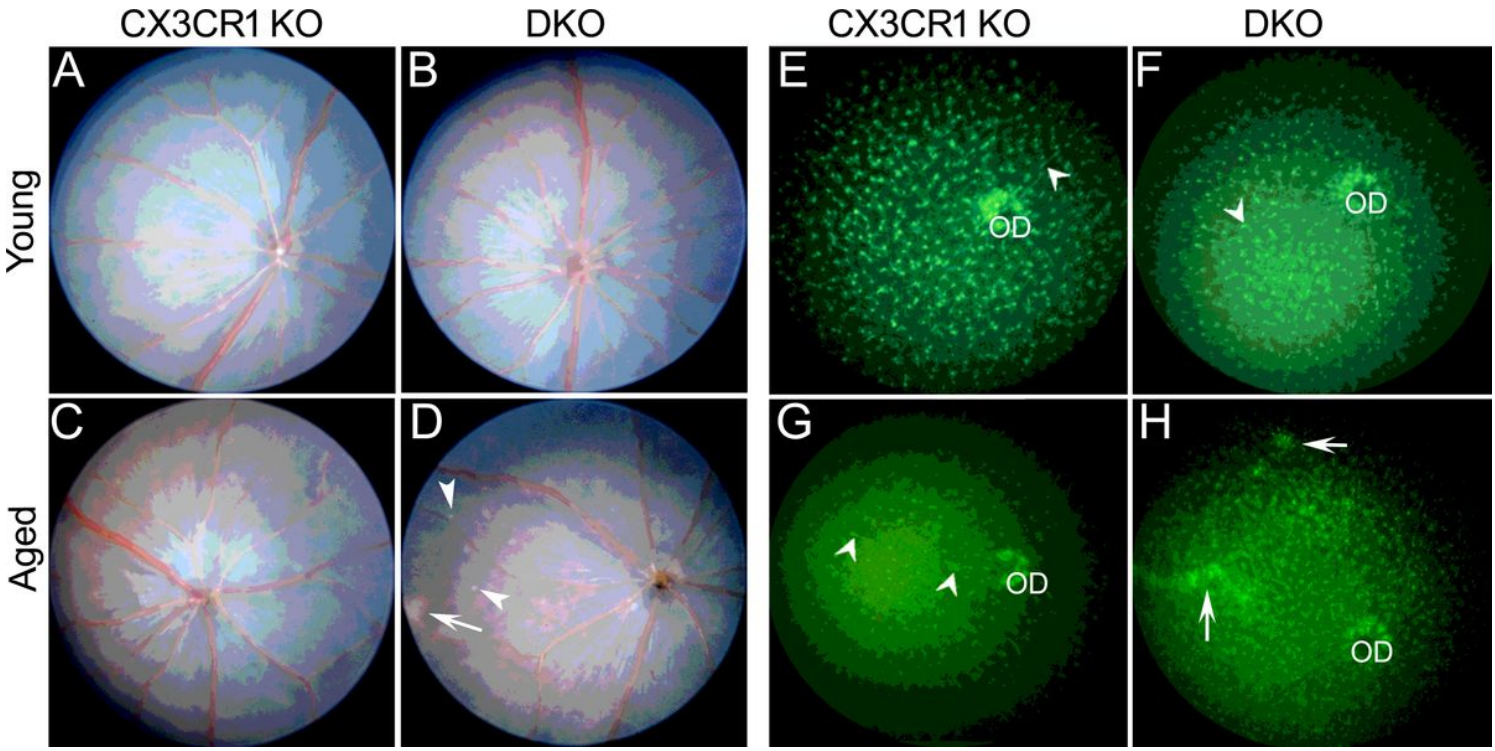

Figure 1

Fundus images and green fluorescence images of Cx3cr1gfp/gfp and DKO mice. (A-D) Fundus images were taken using the topic endoscopic fundus imaging (TEFI) system from 3-month old Cx3cr1gfp/gfp (A) and DKO mice (B), or 12-months old Cx3cr1gfp/gfp (C) and DKO mice (D). Arrow – a patch of whitish lesion; arrowheads – multiple whitish dots. (E-H) Fundus green fluorescence images were taken from 3-month or 12-month oldCx3cr1gfp/gfp (E, G) and DKO (F, H) mice using Micron IV. Arrows – patches of GFP aggregations; arrowheads – perivascular macrophages. OD – optic disc.

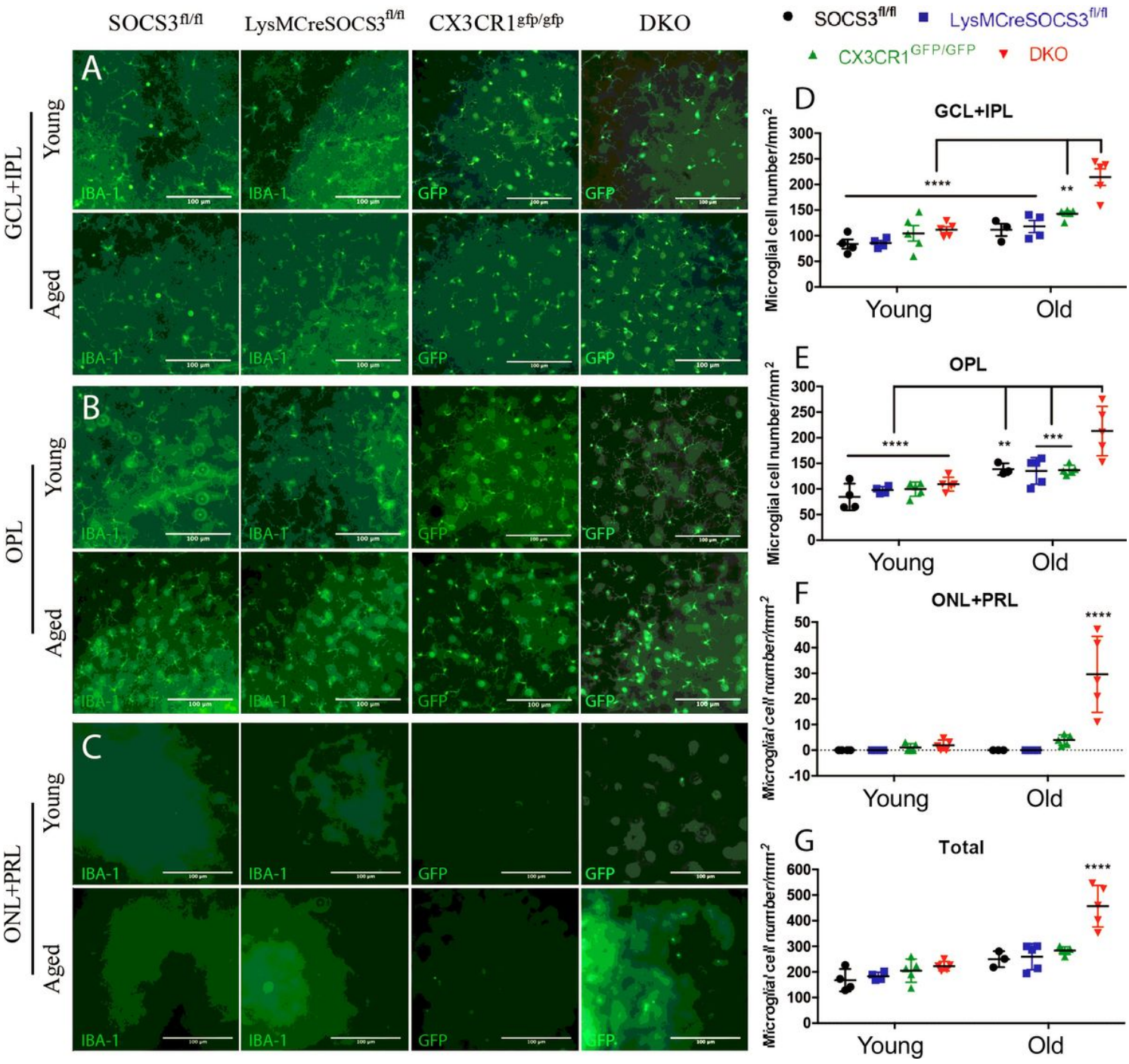

Figure 2

Retinal microglia in different groups of mice. Retinal flatmounts from young (3-5 months) and aged (10-12 months) Socs3fl/fl and LysMCre-Socs3fl/fl mice were stained for IBA-1. Retinal flatmounts from Cx3cr1gfp/gfpand DKO of the same age remain unstained. All samples were imaged by Dmi8 fluorescence microscopy. (A-C) Representative images of retinal microglia from GCL+IPL (A), OPL (B) and ONL+PRL (C). (D-F) quantification of microglia in different retinal layers of different mice. (G) The total number microglia in all retinal layers. Mean ± SD, N = 3~5 mice, Scale bar: 100 μm. Two-way ANOVA, Tukey's test, ** P< 0.01, *** P< 0.001, **** P < 0.0001 (**** showed the difference between aged DKO and

other groups in F and G). GCL – ganglion cell layer; IPL – inner plexiform layer; OPL – outer plexiform layer; ONL – outer nuclear layer; PRL – photoreceptor inner/outer segment layer.

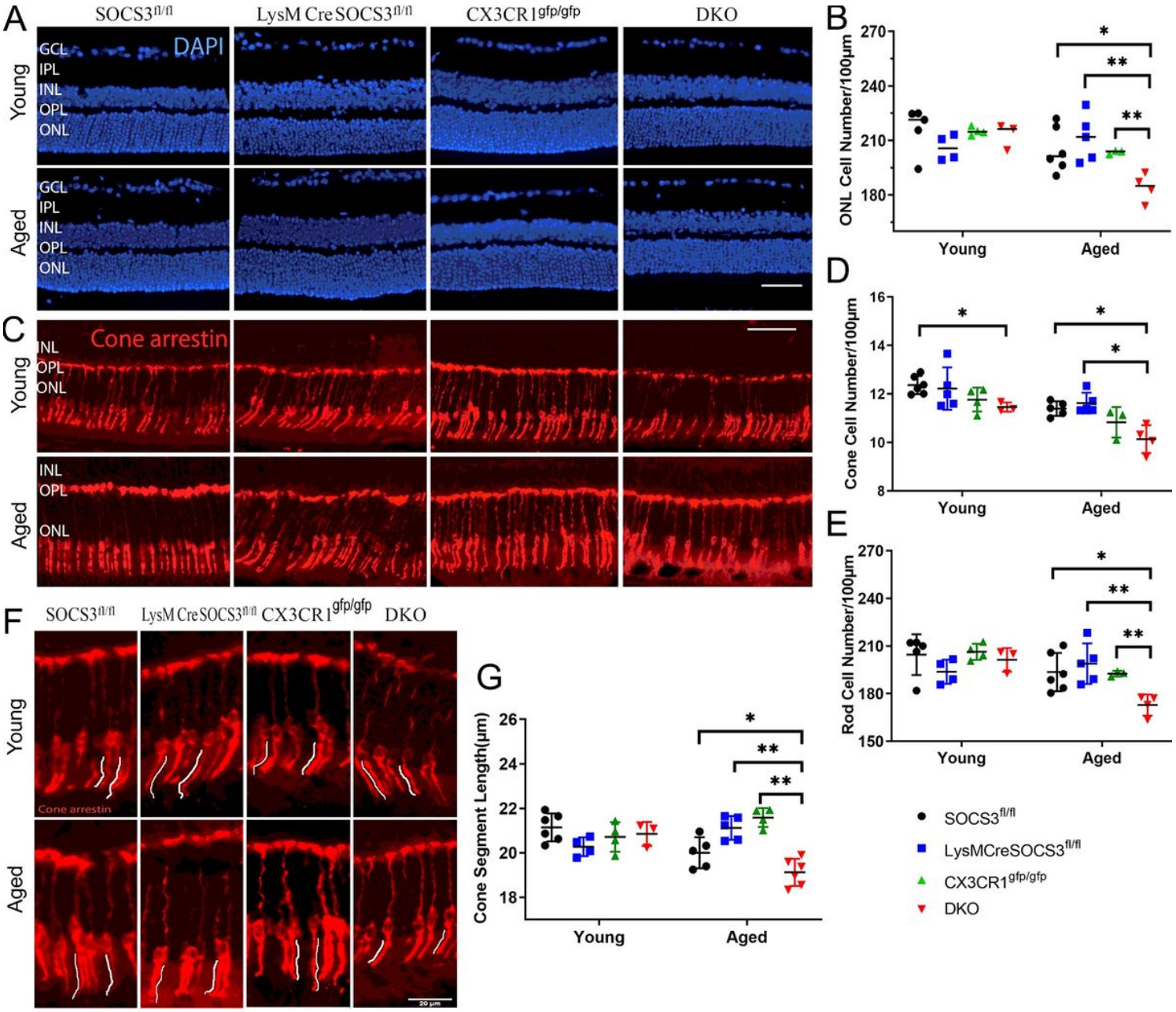

Figure 3

Photoreceptor alterations in different strains of young and aged mice. Retinal sections from young (3-5m) and aged (10-12m) Socs3fl/fl, LysMCre-Socs3fl/fl, Cx3cr1gfp/gfpand DKO mice were stained with DAPI (A) or cone arrestin (C, F) and imaged by Dmi8 fluorescence microscopy. (A) Representative images showing DAPI stained of retinal sections from different groups of mice. (B) Quantitative analysis of DAPI+ cells in ONL in different groups of mice. (C) Representative images of cone arrestin+ cells in retinal sections in different groups of mice. (D) Quantitative analysis of cone arrestin+ cells in different groups of mice. (E) The number of rod cells in different groups calculated by deduction of cone arrestin+ cells from the total number of cells (DAPI+ cells) in the ONL. (F) High magnification images showing inner and outer segments of cone arrestin+ cells in different groups of mice. (G) Quantification of the length of

cone photoreceptorsegments. Mean ± SD; N=3~6 mice. * P <0.05, ** P <0.01, Two-way ANOVA followed by Sidak's multiple comparisons. Scale bar: 50 μm (A, C) or 20 μm (F). GCL – ganglion cell layer; IPL – inner plexiform layer; INL – inner nuclear layer; OPL – outer plexiform layer; ONL – outer nuclear layer.

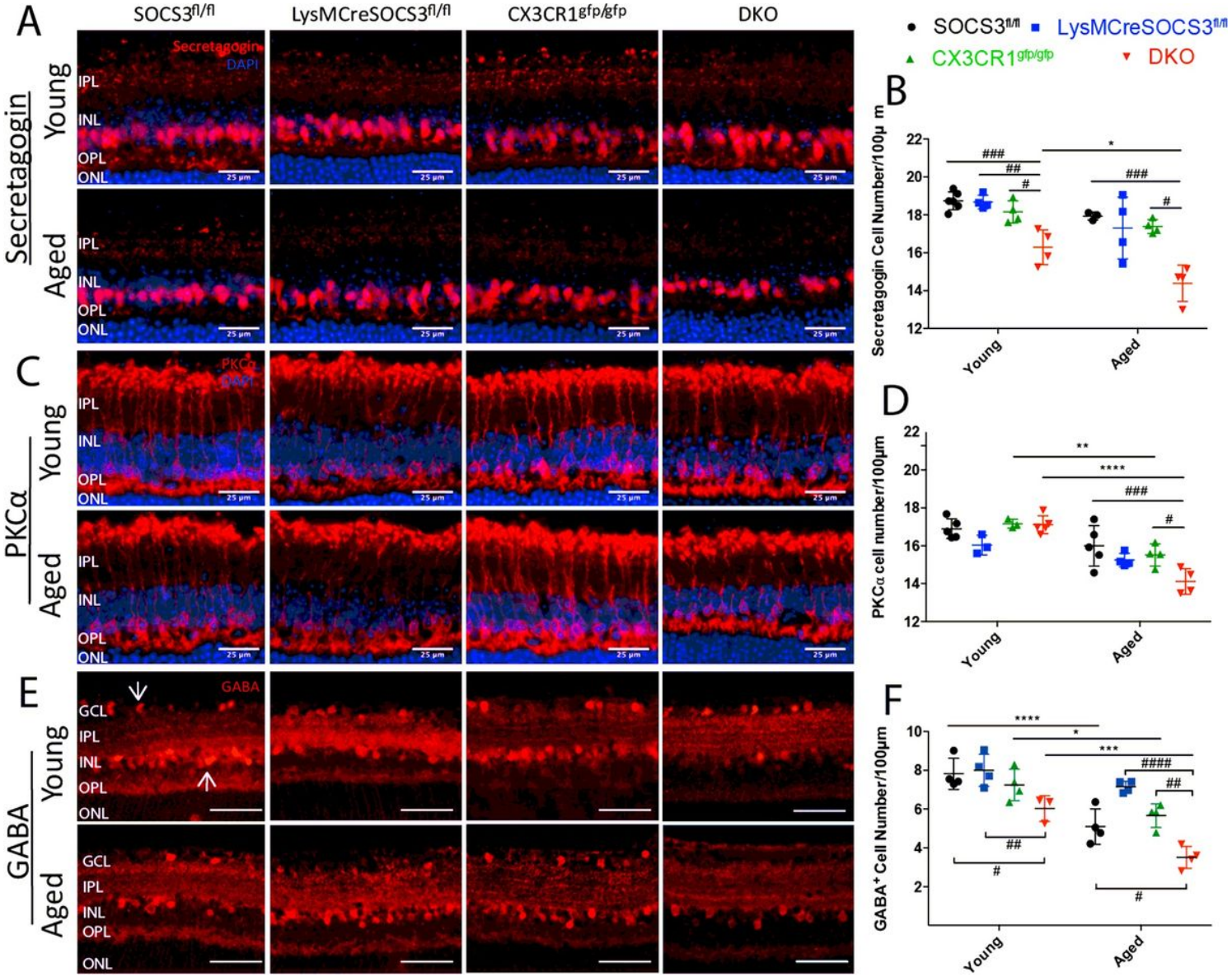

Figure 4

Retinal neurons in different strains of young and aged mice. Retinal sections from young (3-5m) and aged (10-12m) Socs3fl/fl, LysMCre-Socs3fl/fl, Cx3cr1gfp/gfpand DKO mice were stained with secretagogin (A), PKCα (C) and GABA (E) and imaged by Dmi8 fluorescence microscopy. Sections in (A) and (C) were count-stained for DAPI. Quantitative analysis of secretagogin+ (B) and PKCα+ cells (D). (F) Quantitative analysis of GABAergic cells in both GCL and INL (white arrows in E). Scale bar: 25 μm. Mean ± SD, N=3~5 mice, * P < 0.05, ** P < 0.01, *** P < 0.001, **** P < 0.0001; Two-way ANOVA followed by Tukey's test. GCL – ganglion cell layer; IPL – inner plexiform layer; INL – inner nuclear layer; OPL – outer plexiform layer; ONL – outer nuclear layer.

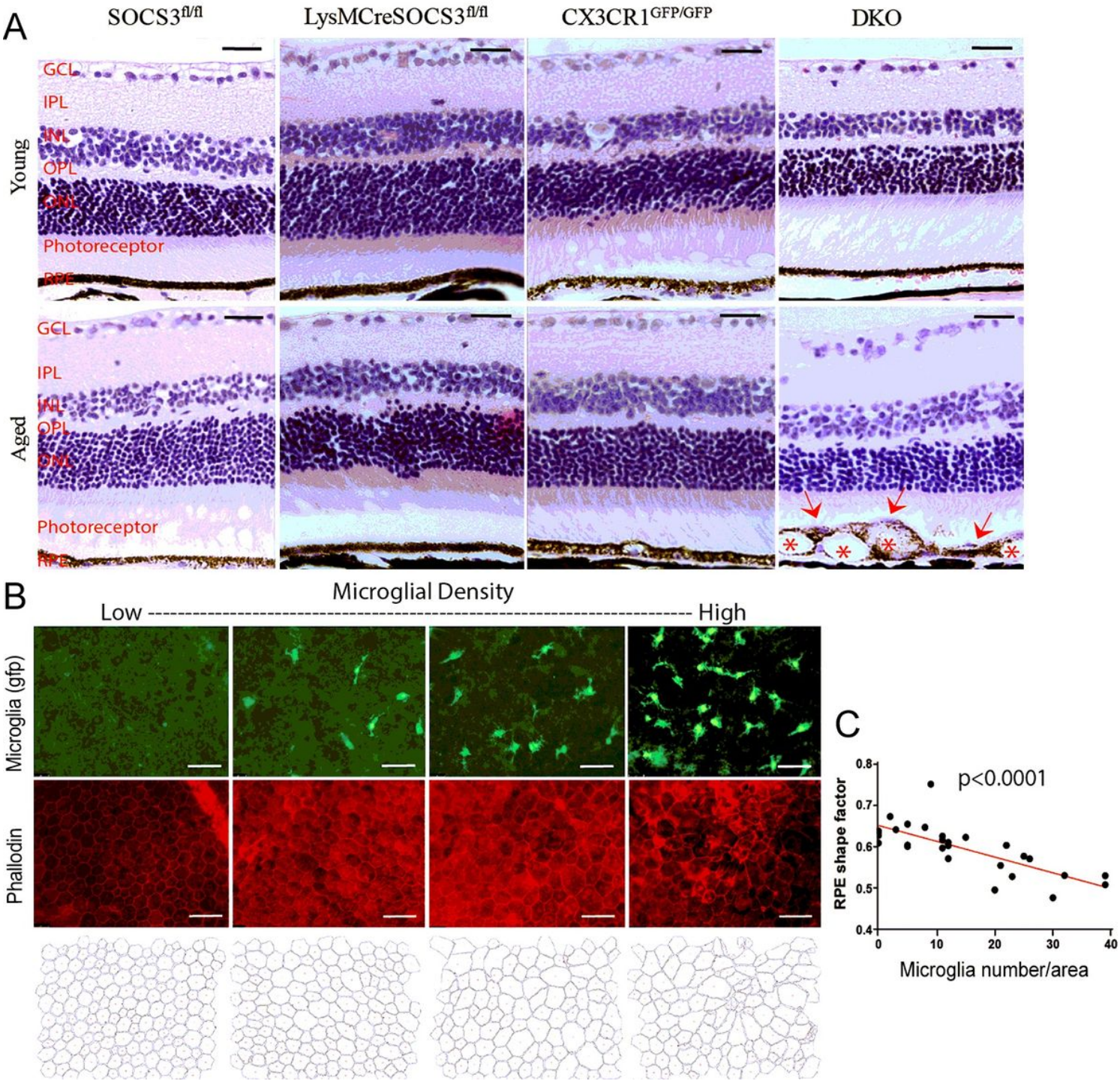

Figure 5

Retinal pigment epithelial cell alterations in different strains of young and aged mice. (A) Eyes from young (3-5m) and aged (10-12m) Socs3fl/fl, LysMCre-Socs3fl/fl,Cx3cr1gfp/gfpand DKO mice were embedded in paraffin and retinal sections were subjected to haematoxylin and eosin (H&E) staining. Images were taken from the central and mid-peripheral area of the retina. Asterisks – vacuoles inside RPE; Red arrows – Purple stained materials (possibly cell nuclei) on top of RPE. Scale bar: 50 µm. GCL – ganglion cell layer; IPL – inner plexiform layer; INL – inner nuclear layer; OPL – outer plexiform layer; ONL – outer nuclear layer; RPE – retinal pigment epithelium. (B) RPE/choroidal flatmounts from 10-12 months

old DKO mice were stained for phalloidin (red) and imaged by Dmi8. GFP+ infiltrating subretinal cells (macrophages or microglia) were in green. Representative images showing areas of normal RPE morphology with no infiltrating cells and different grades of RPE dysmorphologies with different numbers of infiltrating GFP+ cells. The outlines of individual RPEs were sketched at the bottom using FIJI. Scale bar: 50μm. (C) Correlation between RPE shape factor and the number of infiltrating GFP cells. Statistics were applied by five images per mouse from six aged DKO mice.

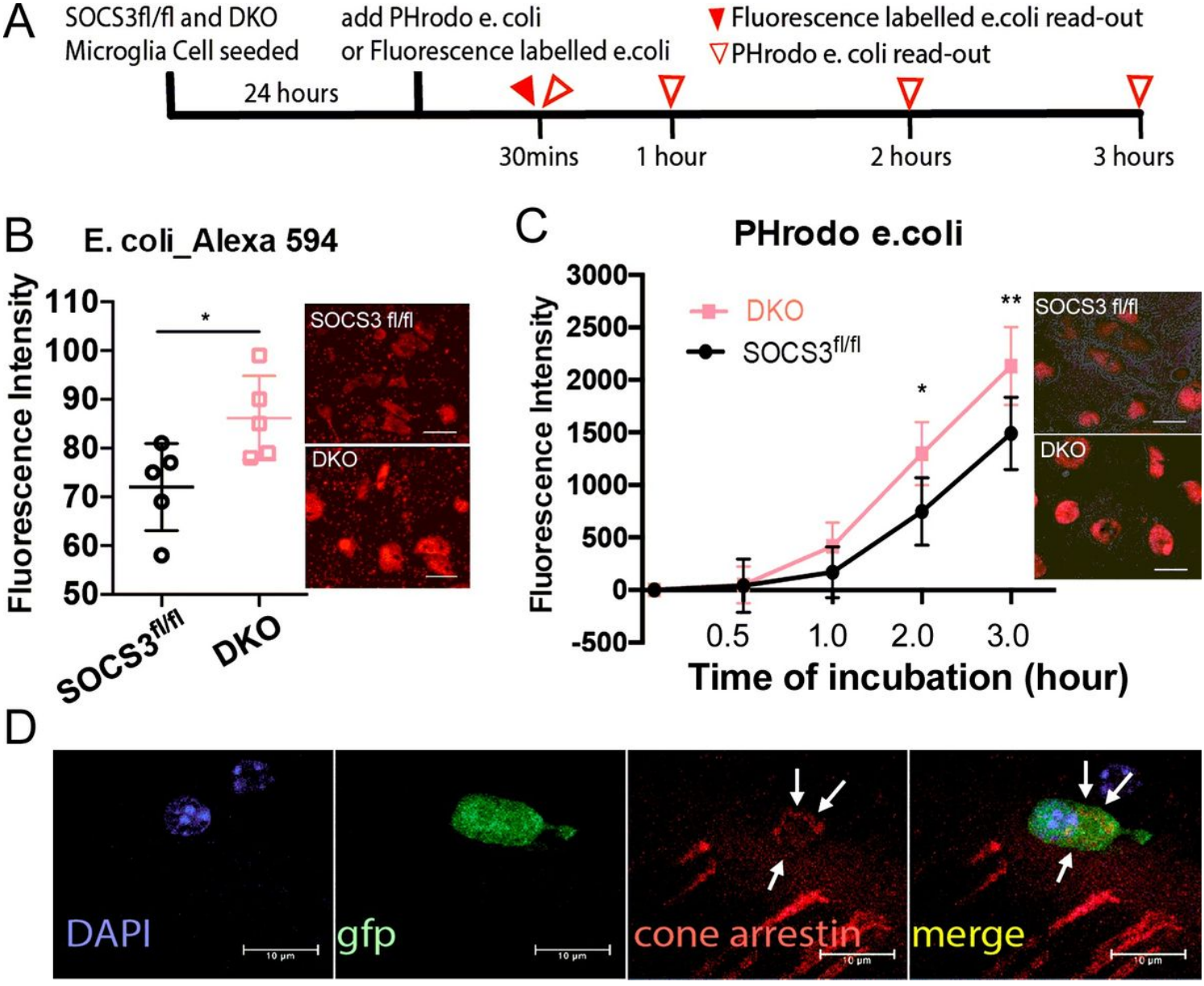

Figure 6

Phagocytic activity of microglia from Socs3fl/fland DKO mice. Two types of phagocytosis assays were conducted as indicated in the schematic diagram (A).(B) Fluorescence conjugated Alexa Fluor E.coli particles were added to microglia and the fluorescence intensities were measured using Fluostar Omega microplate reader and images were taken by Dmi8 fluorescence microscopy 30 minutes later. (C) The pH sensitive E.coli particles were added to microglia. Fluorescent intensities were measured using the microplate reader at 0.5h, 1h, 2h, and 3h later. Images were taken at 3h after incubation using Dmi8. (D)

Images from aged DKO eye section showing cone arrestin antigens (white arrows) inside a GFP+ filtrating cell. Mean ± SD, N=5 (B) and 3 (C).*P<0.05, **P<0.01. Independent sample t test (B); Two-way ANOVA followed by Turkey's test (C). Scale bar: 10 μm.

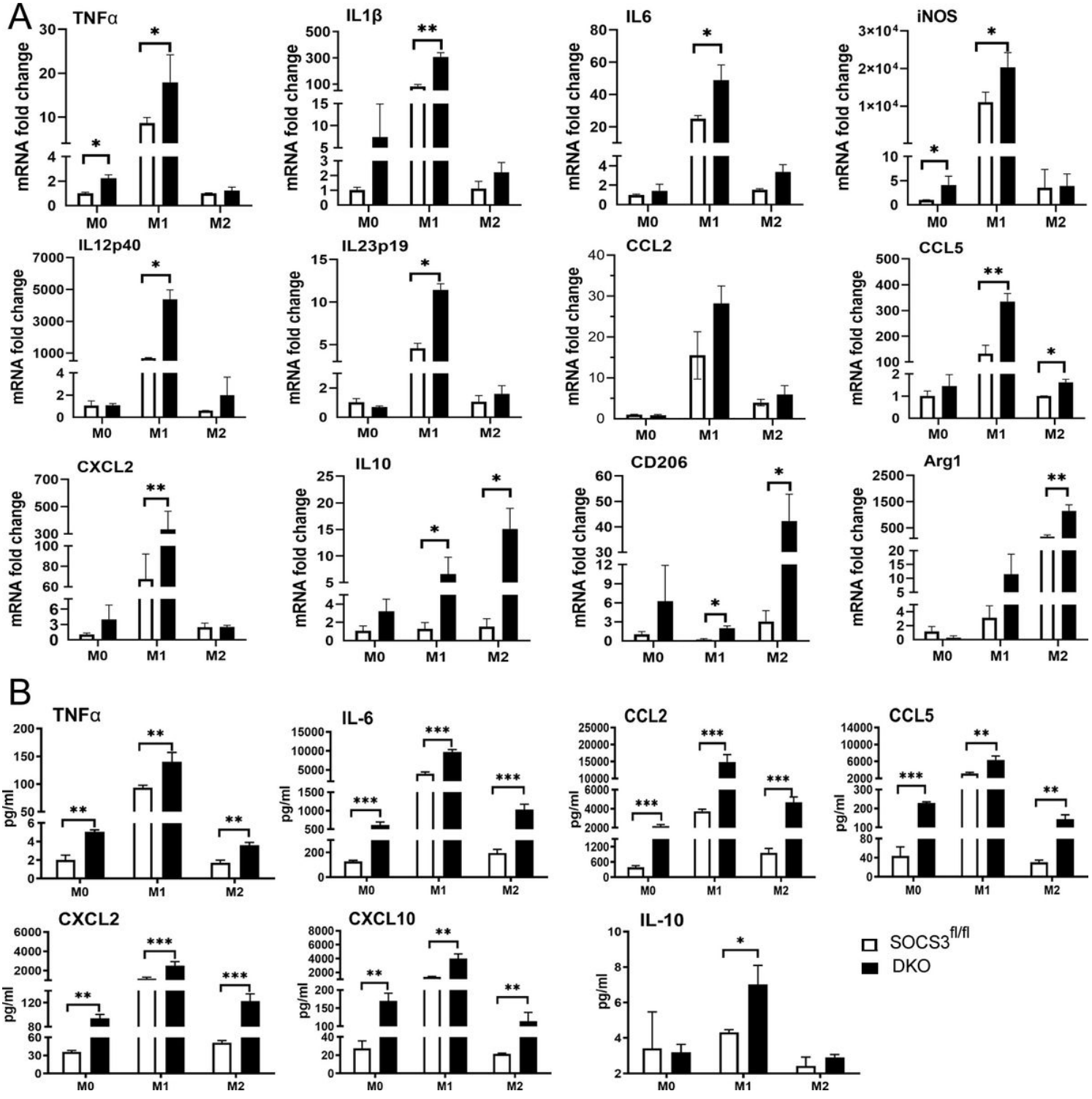

Figure 7

The expression and production of cytokines and chemokines by microglia from Socs3fl/fland DKO mice. Brain microglia from Socs3fl/fland DKO mice were untreated (M0, naive microglia) or treated with LPS+IFNγ(M1) or IL-4 (M2). The mRNA expression of TNF-α, IL-1β, IL-6, iNOS, IL-12p40, IL-23p19, CCL2,

CCL5, CXCL2, IL-10, CD206 and Arg1 were examined by real-time RT-PCR (A). The protein levels of TNF-α, IL-6, CCL2, CCL5, CXCL2, CXCL10 and IL-10 in the supernatants were measured using the cytokine Luminex multiple assay (B). Mean ± SD, N = 3. * P<0.05; ** P<0.01; *** P<0.001. Two-way ANOVA followed by Tukey's multiple comparisons. Experiments were repeated three times.

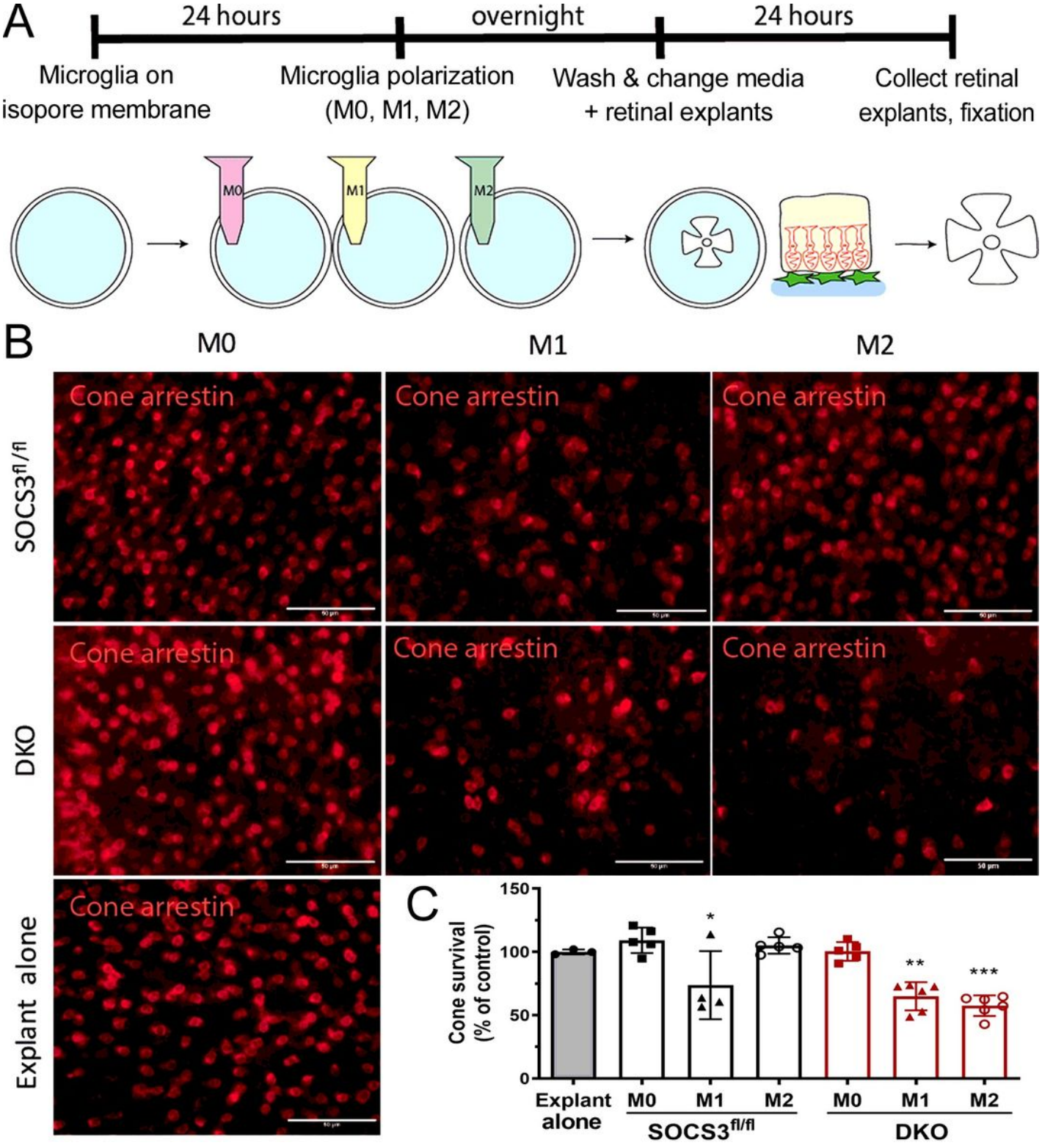

Figure 8

The effect of microglia from Socs3fl/fland DKO mice on photoreceptor survival in retinal explant cultures. Brain microglia were cultured from Socs3fl/fland DKO mice. Retinal explants were from Socs3fl/flmice. Retinal explants were co-cultured with different types of microglia for 24h. The flatmounts of retinal explants were then stained for cone arrestin and imaged by Dmi8 fluorescence microscopy. (A) Schematic diagram showing study design. (B) Representative images showing cone arrestin+cells in retinal explants in different treatment groups. (C) Quantitative data of cone arrestin+ cells in different groups. The number of cone arrestin+ cells in different treatment groups was compared to retinal explants without microglia co-culture. Mean ± SD. N=3~6 explants. * P<0.05, ** P<0.01, *** P<0.001.Two-way ANOVA followed by Tukey's multiple comparisons. Scale bar: 50 μm.

Supplementary Files

This is a list of supplementary files associated with this preprint. Click to download.

- DKOPaperAdditionalFilesV0.docx